Huchon, P., Taylor, B., and Klaus, A. (Eds.)
Proceedings of the Ocean Drilling Program, Scientific Results Volume 180

22. Data Report: Hydrologic Characteristics of Shallow Marine Sediments of Woodlark Basin, Site 1109[1]

S.C. Stover,[2,3] E.J. Screaton,[4] W.J. Likos,[5] and S. Ge[2]

ABSTRACT

Vertical permeability testing was conducted on four samples collected from Site 1109, a borehole advanced during Ocean Drilling Program Leg 180. Closed conditions were applied during each test, and the samples were measured using a constant flow approach and permeant solutions that matched the geochemistry of nearby interstitial waters. Vertical permeabilities measured at 34.5 kPa effective stress generally decreased with depth and ranged from 10^{-14} m^2 at 212.53 meters below seafloor (mbsf) to 10^{-18} m^2 at 698.10 mbsf. The three deepest samples differed in permeability by less than one order of magnitude. Reconsolidation testing on the shallowest sample yielded a minimum permeability of 1.56×10^{-16} m^2 at 276 kPa effective stress. Subsequent rebound testing yielded a hysteresis-type curve, with the final permeability measuring lower than the initial permeability by nearly 1.5 orders of magnitude. Dilution experiments indicated that use of a permeant solution matching the geochemistry of the interstitial waters may be necessary for accuracy in measurements and mitigation of clay swellage and collapse during testing, but further research is mandated.

INTRODUCTION

Knowledge of the permeability of shallow marine sediments is important to our understanding of hydrodynamic and geomechanical

[1]Stover, S.C., Screaton, E.J., Likos, W.J., and Ge, S., 2001. Data report: Hydrologic characteristics of shallow marine sediments of Woodlark Basin, Site 1109. *In* Huchon, P., Taylor, B., and Klaus, A. (Eds.), *Proc. ODP, Sci. Results,* 180, 1–22 [Online]. Available from World Wide Web: <http://www-odp.tamu.edu/publications/180_SR/VOLUME/CHAPTERS/168.PDF>. [Cited YYYY-MM-DD]
[2]University of Colorado, Campus Box 399, Boulder CO 80309, USA. Correspondence author: **stovers@bp.com**
[3]bp, 200 Westlake Park Blvd., WL4/Office 832, Houston TX 77079, USA.
[4]University of Florida, 241 Williamson Hall, PO Box 112120, Gainesville FL 32611, USA.
[5]Colorado School of Mines, Civil Engineering, Golden CO 80401, USA.

Initial receipt: 6 December 2000
Acceptance: 6 June 2001
Web publication: 30 August 2001
Ms 180SR-168

phenomena in marine settings <1 km below the seafloor. In this study, we measure the vertical permeabilities in shallow marine samples extracted from Site 1109, a borehole advanced on the Woodlark Rise during Ocean Drilling Program (ODP) Leg 180. The borehole was advanced to 802 meters below seafloor (mbsf), and the samples in this study range from 212.53 to 698.10 mbsf, thereby allowing for a distribution of permeabilities with depth to be determined. Sediments recovered at this site revealed porosity profiles that deviated from an exponential decrease with depth, potentially indicating overpressure control on the compaction history (Fig. F1A) (Shipboard Scientific Party, 1999a, 1999b). Measurement of permeabilities at this site thus plays a particularly important role in constraining the geomechanical evolution of the sediments and evaluating the role of undercompaction.

We conducted the vertical permeability tests under closed conditions (i.e., the tubing, pressure panel, permeameter, and flow pump were sealed as one system and isolated from any interaction with the environment) using a flow pump to apply a constant low-gradient flow to a flexible wall permeameter system. Because clay swellage and collapse can alter the sample permeability, we avoided such occurrences by creating permeant water solutions that matched the shipboard geochemistry measurements of interstitial waters nearest in depth to those samples investigated in this study. Likewise, we reduced calcite dissolution in the samples through deaerating each permeant solution prior to testing. We also tested the importance of using permeant solutions that simulate known pore water compositions and the influence of increasing and decreasing effective stress on permeability.

F1. Porosity and bulk density profiles, p. 9.

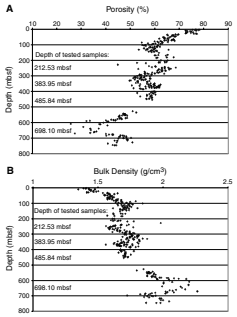

EXPERIMENTAL METHODS

Sample Origin and Transport

Seven whole-round samples were collected from Site 1109, located 11 km north of a south-dipping normal fault system on the Woodlark Rise. Four of these whole rounds were selected at representative depths of 212.53 mbsf (Sample 180-1109C-23X-4, 43–65 cm), 383.95 mbsf (Sample 180-1109D-4R-5, 105–125 cm), 485.84 mbsf (Sample 180-1109D-15R-2, 68–88 cm), and 698.10 mbsf (Sample 180-1109D-38R-2, 112–132 cm) and measured for vertical permeability. The lithologies of the tested cores ranged primarily from clayey silt and silty clay to silty claystone and clayey siltstone (Table T1). Average measured porosities of the tested cores varied from 63.1% to 48.8%, and bulk densities ranged from 1.64 to 1.92 g/cm³ (Table T1; Fig. F1). To preclude moisture loss, each sample was maintained as collected shipboard, encased in plastic sheathing with the ends wax sealed. Furthermore, the samples were refrigerated under humid conditions until the onshore laboratory experiments were initiated.

T1. Description of tested samples, p. 16.

F2. Laboratory setup for vertical permeability testing, p. 10.

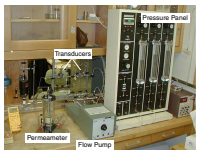

Experiment Design

System Design and Preparation

We used a closed system for permeability testing, consisting of a Harvard Apparatus constant flow pump, a Trautwein M100000 pressure control panel, two Validyne DP15 differential pressure transducers, and a Trautwein flexible wall permeameter (Figs. F2, F3). The system was at-

F3. Constant-flow closed system used in permeability measurements, p. 11.

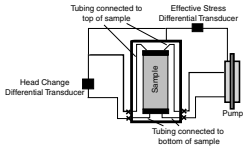

tached to a digital interface for instantaneous readout of effective stress, hydraulic head, and time duration of each test run. Before the experiment, the system was saturated and tested for full closure through applying pressure across the transducers and subsequently monitoring any pressure loss. Likewise, the membrane in the permeameter was tested for reliability.

The constant flow pump was used to generate a constant rate of flow, Q (in cubic meters per second), and a low hydraulic gradient across each sample. The flow could be applied from the bottom of the sample to the top, or reversed in direction, with the constant flow rate maintained for both scenarios. By monitoring the pressure loss across the sample with a differential pressure transducer, the change in head, Δh (in meters), was determined. Using measurements of the sample diameter (in meters), the sample area, A (in square meters), was established and hydraulic conductivity, K (in meters per second), was calculated through Darcy's Law:

$$Q = -KA(\Delta h / \Delta l),$$

where

Δh = the change in head, and
Δl = the measured length of the sample.

Hydraulic conductivity measurements on each sample were conducted until a minimum of four conductivity values were measured at an effective stress of 34.5 kPa, and the conductivity was determined to be stable. The measurements were collected for both flow directions for at least two flow rates. The conductivity values were then converted to permeability, k (in square meters), using the following equation:

$$k = (K \times \mu)/(\rho \times g),$$

where

μ = dynamic viscosity (0.871×10^{-3} Pa·s),
ρ = density (1023 kg/m^3), and
g = gravitational acceleration (9.81 m/s^2).

All tabular results are reported in terms of permeability and conductivity, with graphical results presented as permeability.

Similar low-gradient closed-system techniques have been applied to marine sediment analysis (e.g., Bryant and Bennett, 1988; Fisher et al., 1994; Giambolvo et al., 2000) in lieu of more conventional hydrogeological methods that measure inflow and outflow from an induced head gradient. The closed-system technique eliminates many errors associated with testing low-permeability samples. These errors are outlined in detail in Olsen et al. (1985, 1991). However, the most pertinent benefits of such a system for this study are as follows:

1. Manual flow measurements are avoided, and flow rate, Q, is accurately known.
2. Errors from evaporation and manual volumetric measurements associated with conventional systems are eliminated.

3. Low-permeability samples can be measured at rates faster than the conventional methods would allow.
4. Strong gradients, which can alter in situ permeability in low-permeability sediments through seepage-induced consolidation, are not imposed on the tested samples.

Sample Preparation

In a humidity-controlled environment, each whole-round sample was extracted from the wax-sealed casing immediately prior to sampling. Using a wire saw and a lathe, each sample was trimmed to a height and diameter of no less than 2.5 cm. After being measured for dimensions, the sample was directly placed into the flexible wall permeameter and capped with saturated porous disks. The sample was then backpressured incrementally up to 482.65–689.5 kPa, maintaining 34.5 kPa effective stress. This procedure was conducted over a 24-hr period to ensure saturation and follows ASTM Designation D 5084-90 (2000). Saturation was verified by measuring the pore water pressure and cell pressure at discrete time periods and subsequently calculating a B coefficient as follows:

$$B = (\Delta\text{pore water pressure})/(\Delta\text{cell pressure}).$$

The sample was considered to be saturated at $B \geq 0.95$ for the less indurated sample (180-1109C-23X-4, 43–65 cm) and if $B \geq 0.94$ or remained steady with increasing backpressure for the deeper, more indurated samples (180-1109D-4R-5, 105–125 cm; 15R-2, 68–88 cm; and 38R-2, 112–132 cm).

Sample Pore Water Geochemistry

The shipboard analyses of interstitial waters from samples nearest in depth to those studied here were reviewed. To mitigate clay swellage and collapse from cation exchange or osmotic free energy distribution, which could alter the permeability of the sediment, we created permeant solutions that matched the geochemistry of the interstitial waters (i.e., anion and cation distribution, salinity, and ionic strength) (Table T2). Each permeant solution was placed in a Nold DeAerator and was deaerated under a vacuum pressure before use as the constant flow solution for permeability testing. This procedure reduced the dissolved oxygen in the permeant solution, thus reducing the potential for calcite dissolution in the samples, a further process that could alter the ambient permeability.

T2. Permeant solution composition, p. 17.

Effective Stress Testing

All of the initial conductivity measurements were conducted under conditions of 34.5 kPa effective stress. However, the capability of the low-gradient system allowed for a maximum effective stress of 276 kPa to be imposed on the samples. So that we could observe the influence of reconsolidation and the rebound capacity of the sediments, we tested the least indurated sample, 180-1109C-23X-4, 43–65 cm (212.53 mbsf), for permeability under increasing and decreasing stress conditions, using the appropriate permeant solution. Measurements of the change in permeability with increasing effective stress were conducted until a maximum effective stress of 276 kPa was reached.

Dilution Testing

To test our use of a permeant solution that matched interstitial water geochemistry against conventional methods, where distilled or deionized water is often used, repeat testing was conducted on one sample. Upon completion of the reconsolidation and rebound testing on Sample 180-1109C-23X-4, 43–65 cm, deaerated distilled water was flushed through the system. To ensure that the system was saturated with distilled water, both the Trautwein panel and tubing and the permeameter and tubing were flushed with the deaerated distilled water. The effluent was periodically measured for salinity and conductivity, and the results were compared to the baseline values for the deaerated distilled water (Table T3). The Trautwein panel was flushed with distilled water until the effluent from the panel agreed with the conductivity and salinity measurements of the distilled water. A similar procedure was applied to guarantee replacement of the sample pore waters. The sample was flushed with the deaerated distilled water over a 15-hr time period until over a full pore water volume (46.65 cm^3) was extracted as effluent (Table T3). Moreover, the conductivity and salinity of the final sample effluent agreed with that of the distilled water (Table T3). Vertical permeability testing was then repeated as before, using the distilled water as the permeant solution.

RESULTS

Vertical Permeability

The measured samples ranged in depth from 212.53 to 698.10 mbsf, with lithologies, in general, consisting of clayey silt to silty clay in the shallow sample and clayey siltstone to silty claystone in the deeper samples, reflecting increased induration with depth (Table T1). Permeabilities measured at 34.5 kPa effective stress range from a maximum of 10^{-14} m^2 at 212.53 mbsf and generally decrease with depth to a minimum of 10^{-18} m^2 at 698.10 mbsf (Tables T4, T5; Fig. F4). The three deepest samples (180-1109D-4R-5, 105–125 cm; 15R-2, 68–88 cm; and 38R-2, 112–132 cm) have permeabilities that vary by less than one order of magnitude, likely a result of similar lithologies and degree of induration.

We applied a variety of flow rates to each sample during the testing procedure to evaluate the repeatability of the measured permeabilities. The results from our testing indicate that the repeatability is good (Table T4) and that our test results are not a function of flow rate. Moreover, comparison of hydraulic gradients with varying flow rates reveals a linear relationship (Fig. F5), supporting the establishment of Darcy flow for all applied flow rates.

Permeability and Effective Stress

Under conditions of increasing effective stress, we found that the shallow sample (180-1109C-23X-4, 43–65 cm), collected from 212.53 mbsf, approached a permeability asymptote at nearly 276 kPa effective stress and the permeability decreased by two orders of magnitude (Table T6; Fig. F6). The average permeability measured at 276 kPa effective stress reflects conditions that more closely approximate in situ stresses,

T3. Dilution test parameters and measurements, p. 18.

T4. Vertical permeability measurements, p. 19.

T5. Summary of permeability results, p. 20.

F4. Distribution of measured vertical permeabilities with depth, p. 12.

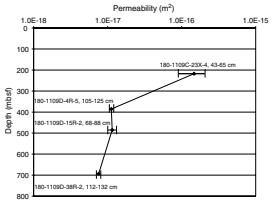

F5. Hydraulic gradients vs. applied flow rates from the low-flow permeability testing, p. 13.

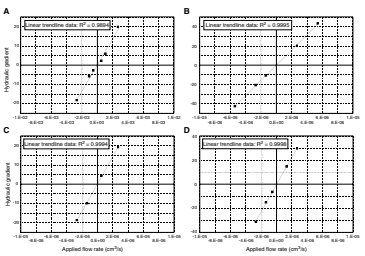

T6. Consolidation and rebound permeability measurements, p. 21.

F6. Permeability response to increasing and decreasing effective stress, p. 15.

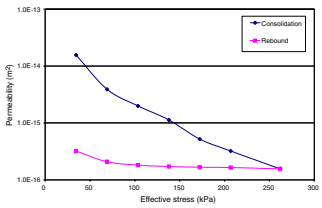

and is thus reported as the permeability in the summary table and figure (Table T5; Fig. F4).

Sample 180-1109C-23X-4, 43–65 cm, was also subject to rebound testing. Results from this study indicate that the permeability follows a hysteresis-type curve with decreasing effective stress (Table T6; Fig. F6). The permeability at the baseline effective stress of 34.5 kPa is nearly 1.5 orders of magnitude less than the original permeability measured under the same conditions.

Sensitivity of Pore Water Geochemistry

Permeability tests were conducted on Sample 180-1109C-23X-4, 43–65 cm (212.53 mbsf), using both the solution matching the interstitial water geochemistry and distilled water. The dilution test was initiated directly after the effective stress test, and the permeability associated with the original permeant solution was extracted from the 34.5-kPa measurement in the rebound test (3.21×10^{-16} m^2) (Table T6). The permeability measured at 34.5 kPa with distilled water as the permeant solution was 2.00×10^{-16} m^2. Although this measurement differs from the baseline permeability by 1.21×10^{-16} m^2, it falls within two standard deviations of the original measurement. Moreover, during the dilution test, we were only able to collect one measurement due to an inconsistent steady-state during the other test runs.

DISCUSSION

Sediment permeability is a governing factor for fluid flow, and hence excess pressure development, in many geological settings (e.g., Bredehoeft and Hanshaw, 1968; Neuzil, 1995). The permeabilities measured in this study approach values believed to be sufficiently low to restrict fluid flow (e.g., Bredehoeft and Hanshaw, 1968; Neuzil, 1995) and, thus, may support overpressure development and influence the porosity profiles observed at Site 1109. Yet, one-dimensional numerical modeling studies of sediment consolidation and pressure development at Site 1109 using the measured permeability values have not shown excess pressure development in the sediments (Stover et al., 2000, submitted [N1]). Further investigation is thus warranted in two and three dimensions to capture the multidimensional physical processes controlling the fluid flow. In conjunction with such studies, the permeability measurements presented here can aid in constraining the influence of low-permeability sediments on the compaction history at Site 1109.

The results from the reconsolidation and rebound tests, however, suggest that the vertical permeability measurements should be viewed in the context of the limitations associated with our procedure. The initial set of permeability values were determined from tests conducted under an effective stress of 34.5 kPa, which differs significantly from the maximum effective stress conditions of each sample prior to being extracted from depth at Site 1109 (Table T5). The sample collected from 212.53 mbsf yielded a permeability decrease exceeding two orders of magnitude with increasing effective stress. The implications for the reconsolidation and rebound testing can be incorporated into numerical modeling of poroelastic materials that use empirically based curves. However, when applying the permeabilities measured under 34.5 kPa effective stress as an estimate for in situ conditions, one should con-

sider that the permeability measurements are likely higher than in situ permeabilities, especially for the shallower, less indurated samples.

During dilution testing on Sample 180-1109C-23X-4, 43–65 cm, use of distilled water as the permeant solution yielded a permeability 38% lower than the initial measurement but which fell within the two standard deviation error bars for the measurement procedures. However, it should be noted that for samples of permeability similar to Sample 180-1109C-23X-4, 43–65 cm, an average flushing rate and sampling run time will allow for multiple volumetric flushings and, thus, pore water replacement (Posey-Dowty et al., 1986) in the sample. As such, depending upon the accuracy needed in the measurements, the lithology and permeability of the sample, and the testing flow rate, use of measured interstitial water geochemistry may be more appropriate in the sample procedure than conventional methods that use distilled or deionized water. In the context of this report, considering that the permeability difference between the compared measurements is not well constrained and only one measurement was extracted, further testing of the necessity of matching pore water geochemistry is warranted.

SUMMARY

The four samples tested in this study yielded permeability values that generally decreased with depth. The shallow sample (180-1109C-23X-4, 43–65 cm) displayed fairly unconsolidated behavior during the reconsolidation and rebound effective stress testing and exhibited the highest permeability of all the samples. The permeabilities of the deeper samples all ranged within the same order of magnitude, likely a result of similar lithologies and a higher degree of induration than the shallow sample. Our experiments also indicate that use of permeant solutions matching the geochemistry of the interstitial waters may be necessary for accuracy in permeability measurements, but further testing is warranted.

ACKNOWLEDGMENTS

The authors would like to thank the Ocean Drilling Program for the Leg 180 Site 1109 samples used in this study. Thanks are also given to Dr. Ning Lu for the gracious use of his engineering lab and equipment at the Colorado School of Mines and Dr. Hal Olsen for his assistance and discussions about the testing procedures. Dr. Kathryn Nagy and Bradley Wakoff offered laboratory and technical support for the pore water geochemistry component of the study. Financial support was provided to S. Chereé Stover through JOI/USSSP postcruise grant 0998.40.1139B. Further JOI/USSSP support was provided to Elizabeth J. Screaton.

REFERENCES

ASTM, 2000. Standard test method for measurement of hydraulic conductivity of saturated porous materials using a flexible wall permeameter. In *Annual Book of ASTM Standards* (Vol. 4.08): West Conshohocken, Penn. (Am. Soc. Testing and Mater.), D5084-90:1070–1077.

Bredehoeft, J.D., and Hanshaw, B.B., 1968. On the maintenance of anomalous fluid pressures: 1. Thick sedimentary sequences. *Geol. Soc. Am. Bull.,* 79:1097–1106.

Bryant, W.R., and Bennett, R.H., 1988. Origin, physical and mineralogical nature of red clays: the Pacific ocean as a model. *Geo-Mar. Lett.,* 8:189–249.

Fisher, A.T., Fischer, K., Lavoie, D., Langseth, M., and Xu, J., 1994. Geotechnical and hydrogeological properties of sediments from Middle Valley, northern Juan de Fuca Ridge. *In* Mottl, M.J., Davis, E.E., Fisher, A.T., and Slack, J.F. (Eds.), *Proc. ODP, Sci. Results,* 139: College Station, TX (Ocean Drilling Program), 627–647.

Giambalvo, E.R., Fisher, A.T., Martin, J.T., Darty, L., and Lowell, R.P., 2000. Origin of elevated sediment permeability in a hydrothermal seepage zone, eastern flank of the Juan de Fuca Ridge, and implications for transport of fluid and heat. *J. Geophys. Res.,* 105:913–928.

Neuzil, C.E., 1995. Abnormal pressures as hydrodynamic phenomena, *Am. J. Sci.,* 205:742–786.

Olsen, H.W., Gill, J.D., Willden, A.T., and Nelson, K.R., 1991. Innovations in hydraulic-conductivity measurements. *Transport. Res. Rec.,* 1309:9–17.

Olsen, H.W., Nichols, R.W., and Rice, T.L., 1985. Low gradient permeability measurements in a triaxial system. *Geotechnique,* 35:145–157.

Posey-Dowty, J., Crerar, D., Hellmann, R., and Chang, C.D., 1986. Kinetics of mineral-water reactions: theory, design and application of circulating hydrothermal equipment. *Am. Mineral.,* 71:85–94.

Shipboard Scientific Party, 1999a. Leg 180 summary. *In* Taylor, B., Huchon, P., Klaus, A., et al., *Proc. ODP, Init. Repts.,* 180, 1–77 [CD-ROM]. Available from: Ocean Drilling Program, Texas A&M University, College Station, TX 77845-9547, U.S.A.

————. Site 1109. *In* Taylor, B., Huchon, P., and Klaus, A., et al., *Proc. ODP, Init. Repts.,* 180, 7–34 [CD-ROM]. Available from: Ocean Drilling Program, Texas A&M University, College Station, TX 77845-9547, U.S.A.

Stover, S.C., Ge, S., Screaton, E.J., and Likos, W.J., 2000. One-dimensional consolidation of shallow marine sediments: application of analytical solutions and experimental data to poroelastic and viscoplastic deformation in Woodlark Basin, Papua New Guinea, *EOS Transactions,* AGU, 81:48. (Abstract)

Figure F1. (**A**) Porosity and (**B**) bulk density profiles for Site 1109. Porosities deviate from an exponential decease with depth primarily in the regions of 150–280 and 350–480 mbsf. These regions, because of their correlation with the highest sedimentation rates for the site, are speculated as zones of overpressure (Shipboard Scientific Party, 1999a, 1999b). The depths from which tested samples were collected are noted on the figure.

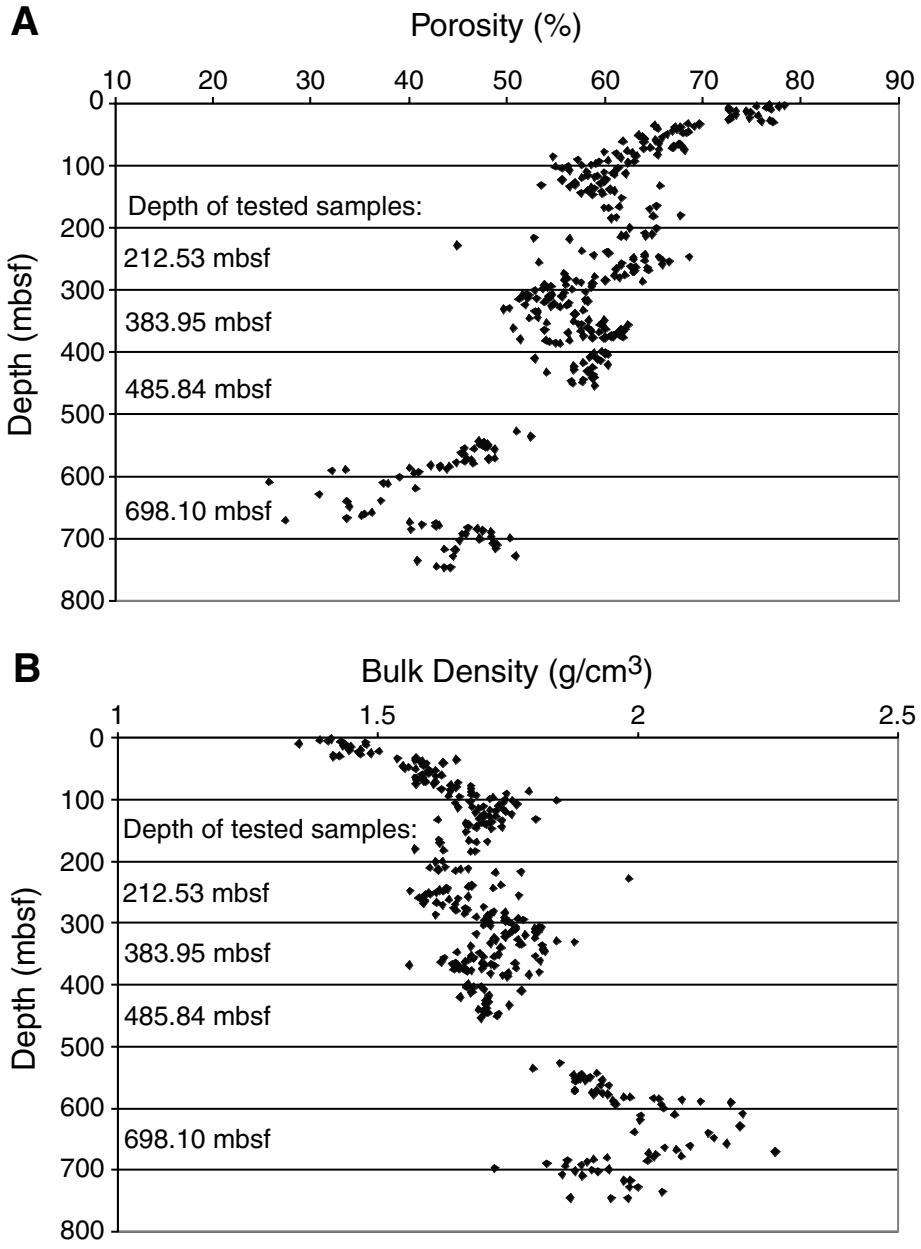

Figure F2. Laboratory setup for vertical permeability testing.

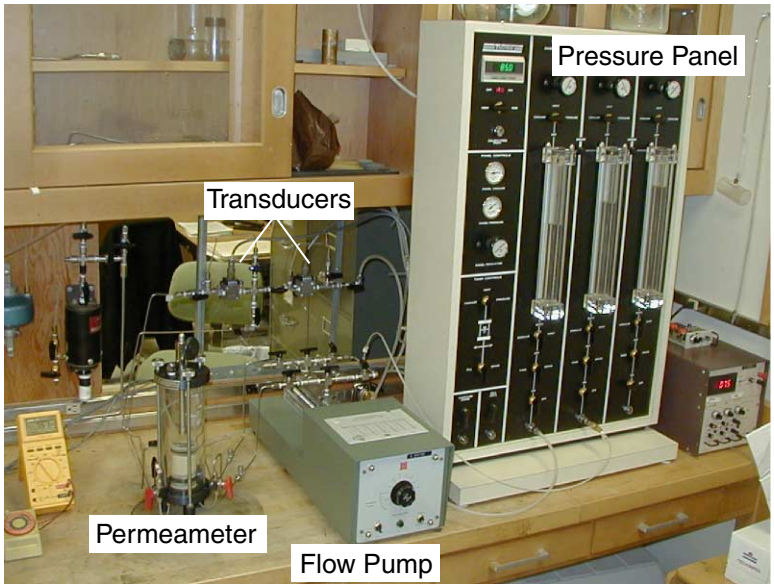

Figure F3. Constant-flow closed system used in permeability measurements. The permeameter cell is connected to a pump that infuses and withdraws permeant water at a constant rate of flow across the sample. Differential pressure transducers measure the pressure difference across the sample (head change) and the pressure difference between the cell fluid and the pore water fluid (effective stress).

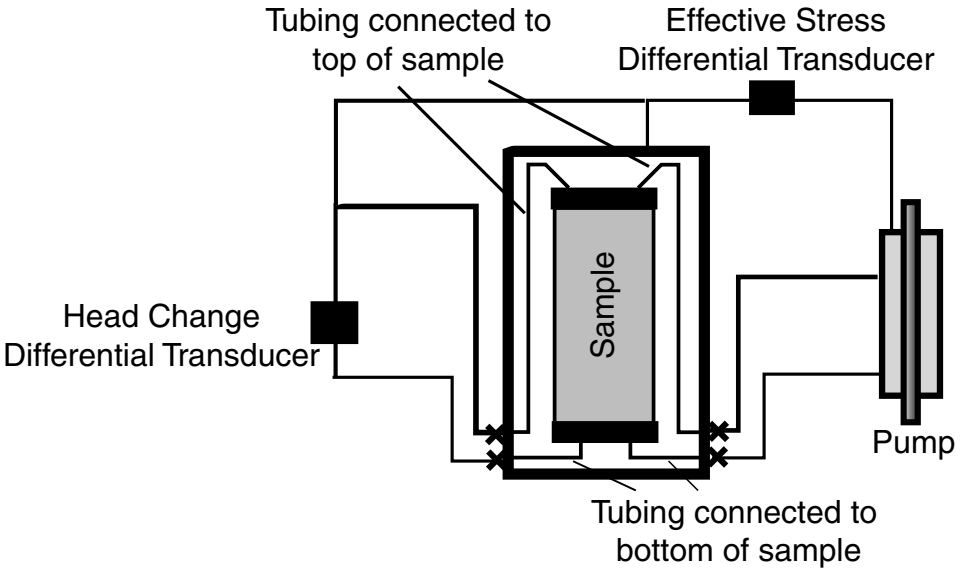

Figure F4. Distribution of measured vertical permeabilities with depth for samples collected from Site 1109. Permeability for Sample 180-1109C-23X-4, 43–65 cm (212.53 mbsf), was measured at an effective stress of 276 kPa, whereas the more indurated samples, 180-1109D-4R-5, 105–125 cm (383.95 mbsf), 15R-2, 68–88 cm (485.84 mbsf), and 38R-2, 112–132 cm (698.10 mbsf), were tested at an effective stress of 34.5 kPa. Error bars represent two standard deviations from the mean permeability measured for each sample.

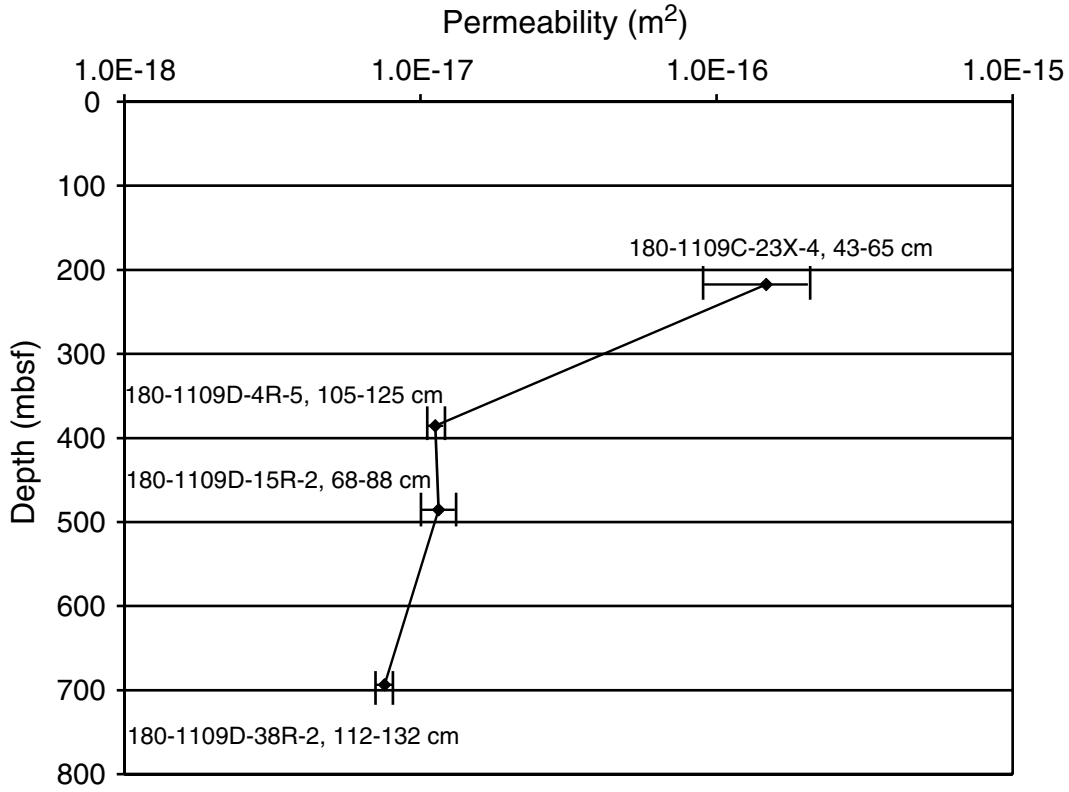

Figure F5. Hydraulic gradients vs. applied flow rates from the low-flow permeability testing on Samples (**A**) 180-1109C-23X-4, 43–65 cm (212.53 mbsf), (**B**) 180-1109D-4R-5, 105–125 cm (383.95 mbsf), (**C**) 180-1109D-15R-2, 68–88 cm (485.84 mbsf), and (**D**) 180-1109D-38R-2, 112–132 cm (698.10 mbsf). The linear relationship indicates that Darcy flow was established in each run, regardless of flow rate. Solid lines represent the linear trend line, and the solid points represent measured hydraulic gradients. The change in sign for flow rate and hydraulic gradient represents a change in flow direction. Negative indicates a flow direction from the top of the sample to the bottom, whereas positive indicates a flow direction from the bottom of the sample to the top. (**Figure shown on next page.**)

Figure F5 (continued). (Caption shown on previous page.)

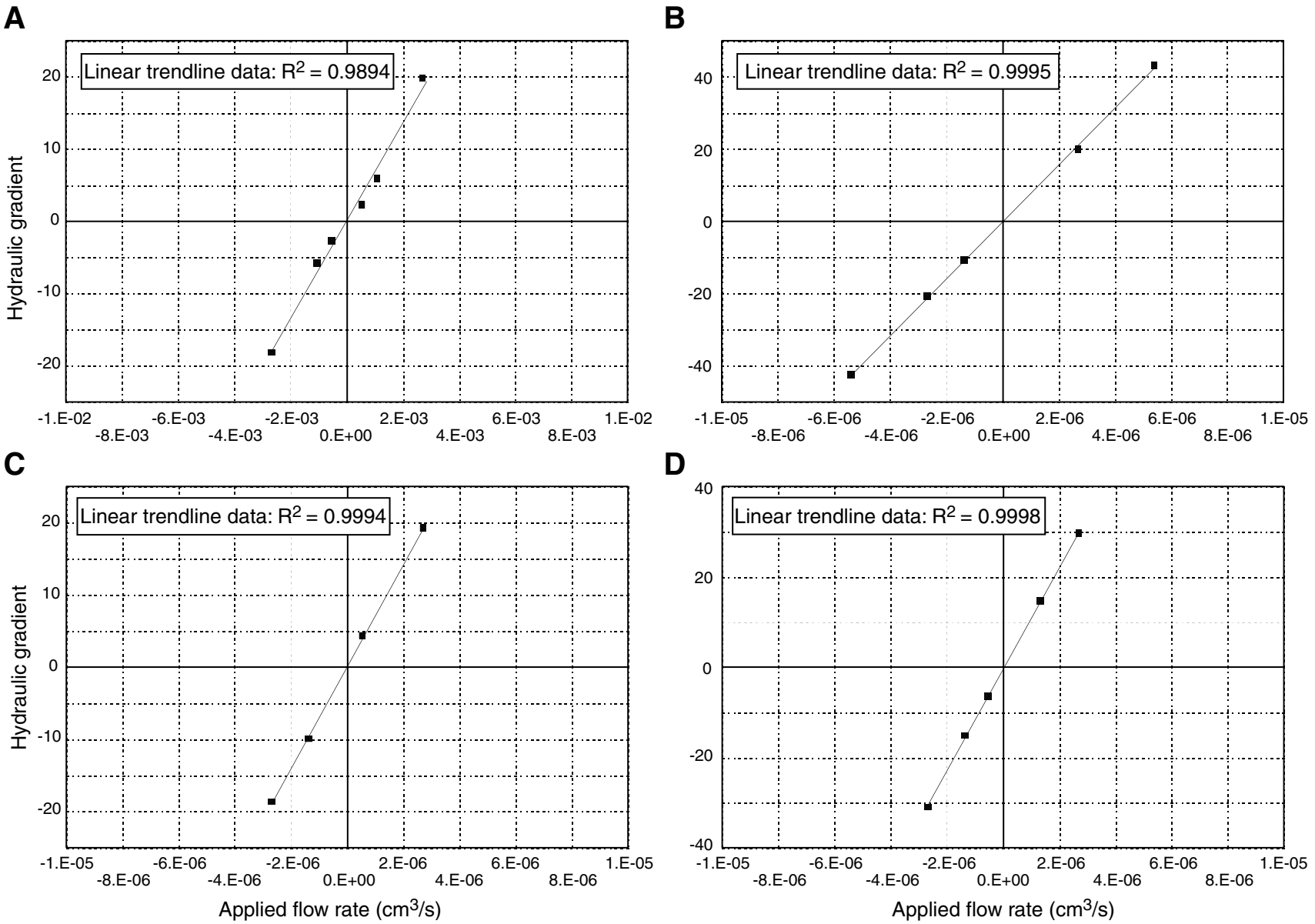

Figure F6. Permeability response to increasing effective stress (reconsolidation) and decreasing effective stress (rebound) for Sample 180-1109C-23X-4, 43–65 cm (212.53 mbsf). Maximum in situ vertical effective stress for this sample is 1.71 MPa.

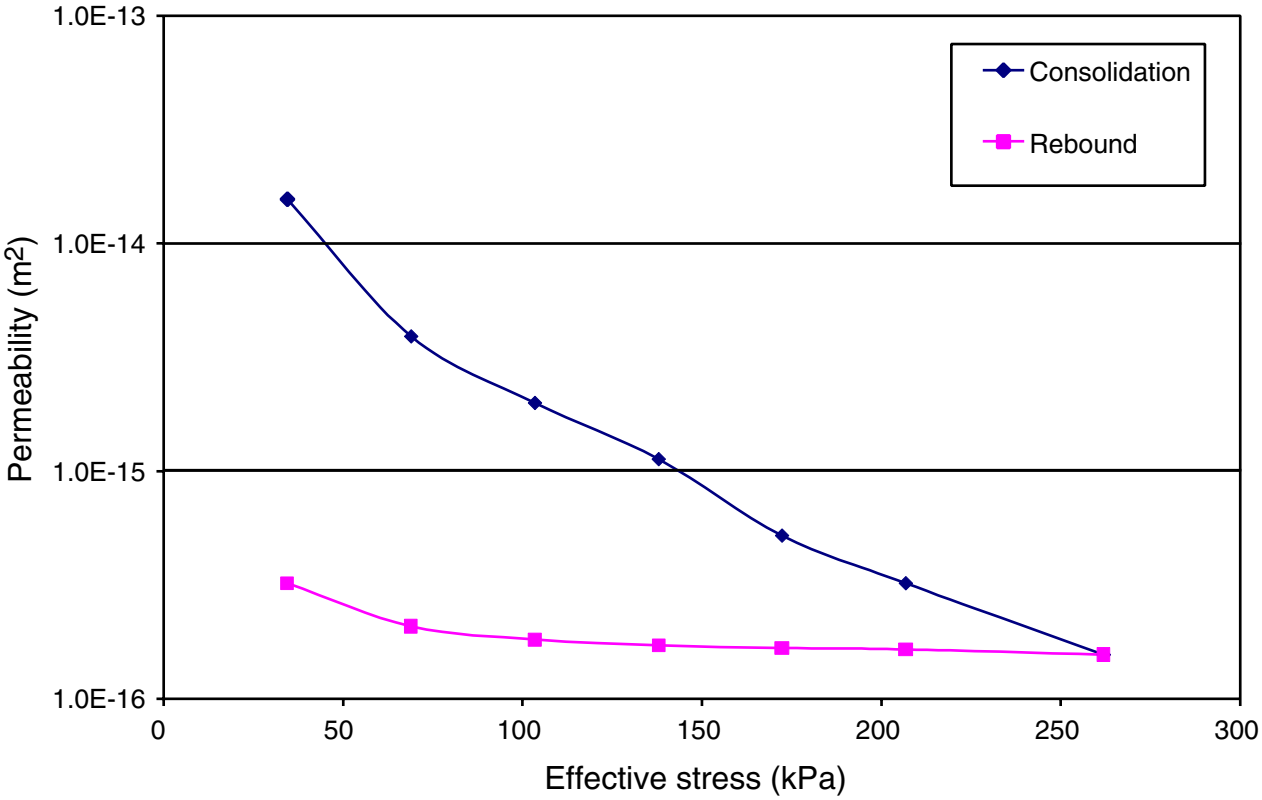

Table T1. Summarized description of tested samples.

Core, section, interval (cm)	Depth (mbsf)	Porosity (%)	Bulk density (g/cm^3)	Lithologic unit	General lithology	Depositional environment	Depositional facies
180-1109C-							
23X-4, 43–65	212.53	63.1	1.64	III	Clayey silt/silty clay interlayered with clayey silt to coarse sand	Mid-bathyal 500–2000 m	Pelagic and hemipelagic silty clays with gravity-flow deposits
180-1109D-							
4R-5, 105–125	383.95	54.6	1.76	V	Clayey siltstone/silty claystone interbedded with volcaniclastic sand	Upper bathyal 150–500 m	Calcareous hemipelagic and possible fine-grained turbidite sediments with turbidity current volcanic deposits
15R-2, 68–88	485.84	54.9	1.77	VI	Clayey siltstone/silty claystone interlayered with clayey siltstone to coarse-grained sandstone	Upper bathyal 150–500 m	Hemipelagic carbonate clay with mainly low-density turbidity current deposits
38R-2, 112–132	698.10	48.8	1.92	VIII	Silty claystone/clayey siltstone	Brackish water	Fine-grained soil deposits in a quiet environment with influx of nearby plant material

Notes: Porosity values are averaged from shipboard measurements of two samples nearest in location to those tested in this study. General lithology, depositional environment, and depositional facies were extracted from the Shipboard Scientific Party (1999b).

Table T2. Geochemistry recipes used to create permeant solutions matching that of nearby interstitial waters.

Core, section, interval (cm)		Core depth (mbsf)		Ionic strength (M)		SO_4	Na	K	Mg	Ca	Li	NH_4	Sr
IW	WR	IW	WR	IW	WR solution	(g Na_2SO_4/L)	(g NaCl/L)	(g KCl/L)	(g $MgCl_2 \cdot 6H_2O$/L)	(g $CaCl_2 \cdot 2H_2O$/L)	(g LiCl/L)	(g NH_4Cl/L)	(g $SrCl_2 \cdot 6H_2O$/L)
180-1109C-	180-1109C-												
23X-4, 33–43	23X-4, 43–65	212.43	212.53	0.6055	0.6031	0.2983	26.8123	0.6113	7.6038	0.7498	0.0008	0.1001	0.0339
180-1109D-	180-1109D-												
4R-3, 96–106	4R-5, 105–125	381.56	383.95	0.5932	0.5862	0.0000	25.4798	0.7231	7.6648	1.2350	0.0013	0.0905	0.0429
14R-4, 136–146	15R-2, 68–88	479.32	485.84	0.5942	0.5911	0.0000	26.0058	0.8350	7.0549	1.3673	0.0021	0.1126	0.0669
38R-4, 140–150	38R-2, 112–132	701.16	698.10	0.6517	0.6567	0.0000	24.2526	0.1267	4.9608	7.9832	0.0022	0.0534	0.2552

Notes: IW = interstitial water, WR= whole-round sample. M = molarity (number of moles of solute/liter of solution).

Table T3. Calculations, assumptions, and measurements applied toward determining sample pore water dilution for the distilled water permeant solution test.

Calculations		
Depth of core (mbsf):	212.53	
Porosity (n) (%)*:	63.10	
Sample volume (V_t) (cm^3):	46.65	
Sample radius (cm):	1.77	
Sample height (cm):	4.74	
Flow rate (cm^3/s):	5.40E–04	
V_{pw} (cm^3):	29.39	
Time for dilution (s):	5.44E+04	
Time for dilution (min):	907.47	
Time for dilution (hr):	15.12	
Measurements	Conductivity (µS/cm)	Salinity (‰)
Distilled water	112.1	0.1
Effluent from Trautwein initial	7.83×10^3	4.6
Effluent from Trautwein final	114.5	0.1
Effluent from sample initial	NA	NA
Effluent from sample final	114.1	0.1

Notes: * = taken from Leg 180 data. Assuming that there are no preferential flow pathways, the volume of pore water (V_{pw}) = $V_t \times n$. NA = not available.

Table T4. Vertical permeability measurements.

Core, sample, interval (cm)	Depth (mbsf)	Length (m)	Diameter (m)	Area (m^2)	Saturation (*B*) (%)	Effective stress (kPa)	Run	Gear	Flow direction	Flow rate (cm^3/s)	Δh (kPa)	Δh (cm H_2O)	Gradient ($\Delta h/\Delta l$)	K (m/s)	k (m^2)
180-1109C-															
23X-4, 43–65	212.53	0.0474	0.0354	0.0010	97	34.5	1	1	b to t	2.70E–03	9.22	93.96	19.82	1.38E–07	1.20E–14
							2	2	b to t	1.08E–03	2.81	28.64	6.04	1.82E–07	1.58E–14
							3	3	b to t	5.40E–04	1.07	10.91	2.30	2.38E–07	2.07E–14
							4	1	t to b	–2.70E–03	–8.43	–85.91	–18.13	1.51E–07	1.31E–14
							5	2	t to b	–1.08E–03	–2.71	–27.61	–5.83	1.88E–07	1.63E–14
							6	3	t to b	–5.40E–04	–1.29	–13.12	–2.77	1.98E–07	1.72E–14
													Average:	1.83E–07	1.59E–14
180-1109D-															
4R-5, 105–125	383.95	0.0424	0.0354	0.0010	94	34.5	1	10	b to t	2.70E–06	8.35	85.14	20.08	1.37E–10	1.19E–17
							2	9	b to t	5.40E–06	18.01	183.64	43.31	1.27E–10	1.10E–17
							3	9	t to b	–5.40E–06	–17.74	–180.91	–42.67	1.29E–10	1.12E–17
							4	10	t to b	–2.70E–06	–8.58	–87.49	–20.63	1.33E–10	1.15E–17
							5	11	t to b	–1.35E–06	–4.46	–45.43	–10.72	1.28E–10	1.11E–17
													Average:	1.31E–10	1.13E–17
15R-2, 68–88	485.84	0.0540	0.0360	0.0010	NA	34.5	1	12	b to t	5.40E–07	2.31	23.60	4.37	1.21E–10	1.05E–17
							2	10	b to t	2.70E–06	10.20	104.05	19.27	1.38E–10	1.19E–17
							3	10	t to b	–2.70E–06	–9.86	–100.54	–18.62	1.42E–10	1.24E–17
							4	11	t to b	–1.35E–06	–5.24	–53.40	–9.89	1.34E–10	1.16E–17
													Average:	1.34E–10	1.16E–17
38R-2, 112–132	698.10	0.0547	0.0360	0.0010	94	34.5	1	9	b to t	5.40E–06	NA	NA	NA	NA	NA
							2	10	b to t	2.70E–06	16.01	163.26	29.85	8.88E–11	7.71E–18
							3	11	b to t	1.35E–06	7.89	80.50	14.72	9.01E–11	7.82E–18
							4	11	t to b	–1.35E.06	–8.06	–82.22	–15.03	8.82E–11	7.66E–18
							5	10	t to b	–2.70E–06	–16.67	–170.02	–31.08	8.53E–11	7.40E–18
							6	12	t to b	–5.40E–07	–3.43	–34.95	–6.39	8.30E–11	7.20E–18
													Average:	8.71E–11	7.56E–18

Notes: Flow direction: b to t = flow from bottom of sample to top, t to b = flow from top of sample to bottom. NA = not available due to poorly resolved steady state. Each test was conducted under an effective stress of 34.5 kPa.

Table T5. Summary of permeability results for ODP Site 1109.

Whole-round sample (cm)	Depth (mbsf)	Average K (m/s)	Average k (m^2)	Porosity (%)	Maximum lithostatic load (MPa)	Maximum effective stress (MPa)
180-1109C-						
23X-4, 43–65	212.53	1.80E–09	1.56E–16	63.1	3.84	1.71
180-1109D-						
4R-5, 105–125	383.95	1.31E–10	1.13E–17	54.6	7.46	3.61
15R-2, 68–88	485.84	1.34E–10	1.16E–17	54.9	9.44	4.56
38R-2, 112–132	698.10	8.71E–11	7.56E–18	48.8	15.49	8.48

Notes: K = hydraulic conductivity, k = permeability. The reported permeability for Sample 180-1109C-23X-4, 43–65 cm, was measured at 276 kPa effective stress, whereas the remainder of the samples were measured at 34.5 kPa and thus represent maximum values.

Table T6. Permeability measurements during consolidation and rebound.

Core, section, interval (cm)	Depth (mbsf)	Run	Effective stress (kPa)	*K* (m/s)	*k* (m^2)
180-1109C-23X-4, 43–65	212.53	1	34.48	1.80E–07	1.56E–14
		2	68.95	4.50E–08	3.91E–15
		3	103.43	2.30E–08	2.00E–15
		4	137.90	1.30E–08	1.13E–15
		5	172.38	6.00E–09	5.21E–16
		6	206.85	3.70E–09	3.21E–16
		7	262.01	1.80E–09	1.56E–16
		8	206.85	1.90E–09	1.65E–16
		9	172.38	1.93E–09	1.68E–16
		10	137.90	1.98E–09	1.72E–16
		11	103.43	2.10E–09	1.82E–16
		12	68.95	2.40E–09	2.08E–16
		13	34.48	3.70E–09	3.21E–16

CHAPTER NOTE*

N1. Stover, S.C., Ge., S., and Screaton, E.J., submitted. A one-dimensional analytically based approach for studying poroelastic and viscoplastic consolidation: application to Woodlark Basin, Papua New Guinea. *J. Geophys. Res.*

*Dates reflect file corrections or revisions.